Atmospheric Research 268 (2022) 106000

Contents lists available at ScienceDirect

Atmospheric Research

journal homepage: www.elsevier.com/locate/atmosres

Combination of PM optical and chemical properties to estimate the contribution of non-BC absorbers to light absorption at a remote site

A. López-Caravaca [a], J.F. Nicolás [a,*], F. Lucarelli [b], R. Castañer [a], J. Crespo [a], N. Galindo [a], G. Calzolai [b], E. Yubero [a], A. Clemente [a], G. Pazzi [b]

[a] Atmospheric Pollution Laboratory (LCA), Department of Applied Physics, Miguel Hernández University, Avenida de la Universidad S/N, 03202 Elche, Spain
[b] Department of Physics and Astronomy, University of Florence and INFN, Sesto Fiorentino, Italy

ARTICLE INFO

Keywords:
High time resolution
Mountain site
Aerosol type classification
Non-BC absorbing components

ABSTRACT

Values of particulate matter (PM) concentrations, chemical composition and aerosol optical parameters have been measured with a high time resolution (1-hour) for thirteen days at the end of summer 2014. Sampling was performed at a remote site (1558 m a.s.l) located in the southeast of the Iberian Peninsula, close to the Mediterranean coast. According to the optical and chemical characteristics of PM, four periods were differentiated using Cluster analysis. One cluster (C4) was clearly associated with Saharan dust inputs. During this period, mineral dust (MD) concentrations were highest. Values of the intensive optical parameters for C4 confirmed that MD was the dominant type of aerosol: AAE (1.58) was the highest of the four periods, while SAE (−0.58) was the lowest. C4 was selected to apply a methodology capable of discriminating the contribution from Black carbon (BC) and Non-BC absorbers (NBC), that is Brown carbon (BrC) and MD, to the light absorption process. With the objective of determining the contribution of NBC to light absorption, the spectral differences between BC and NBC were used. The value of the absorption coefficient for NBC (σ_{ap}-NBC) was plotted versus the concentration of MD. The approach consists on drawing a line including points aligned in the lower end of the chart. The equation of this line can be used to estimate the MD contribution (σ_{Dust}) to light absorption. For $\lambda = 520$ nm, around 6% of the absorption was due to MD and ~ 8% to BrC. This methodology allowed the determination of the MAE (Mass Absorption Efficiency) value for Fine-MD, (0.032 ± 0.004 m^2 g^{-1} for $\lambda = 520$ nm).

1. Introduction

Discriminating different types of aerosols is important in order to understand their role in atmospheric processes. For example, different types of aerosols have different radiative forcing properties (Schmeisser et al., 2017) and can lead to distinct adverse effects on human health (Park et al., 2018).

Identifying the types of aerosols requires knowing their chemical composition and size distribution. Generally, this information can be obtained from chemical analysis of size-resolved particulate matter (PM) collected on filters. However, it can also be inferred from the analysis of aerosol intensive optical properties. Several combinations of optical parameters have been used for this purpose. An illustrative example is the use of the Angström matrix (Cazorla et al., 2013; Cappa et al., 2016) representing the division of the Absorption Angström Exponent (AAE) vs. Scattering Angström Exponent (SAE) space. This approach provides a good discrimination among light-absorbing PM components such as mineral dust (MD), organic carbon (OC) and black carbon (BC) since each of these species have specific and well-known values of AAE and SAE. The use of 3-D schemes has also been frequently applied as they provide a robust visualization and further insights into an aerosol population (Schmeisser et al., 2017). Romano et al. (2019) used the combination of AAE, SAE and d(SSA) (spectral variability of single scattering albedo) to discriminate up to eight different aerosol populations. These parameters, together with the SSA (Single Scattering Albedo), were used by Costabile et al. (2013) to find key aerosol populations that were optically separated at a suburban background site close to Rome (Italy). The same intensive parameters were used by Kaskaoutis et al. (2021) for the categorization of key aerosol groups at an urban background site in Athens (Greece). In the work by Schmeisser et al. (2017), up to three different methods to classify aerosols types (AAE vs. SAE, a multivariate cluster analysis, and relationship between air mass trajectories and intensive optical parameters) can be found. The identification of time periods dominated by different PM components (MD, biomass burning,

* Corresponding author at: Laboratory of Atmospheric Pollution, Miguel Hernández University, Av. de la Universidad s/n, Edif. Alcudia, 03202 Elche, Spain.
E-mail address: j.nicolas@umh.es (J.F. Nicolás).

https://doi.org/10.1016/j.atmosres.2021.106000
Received 10 May 2021; Received in revised form 21 December 2021; Accepted 26 December 2021
Available online 29 December 2021

sea salt, etc..) has also been achieved by combining the study of optical parameters with PM chemical composition (Yang et al., 2009; Valentini et al., 2020).

Whatever the method used, three main light-absorbing PM components are usually identified: Black Carbon (BC), considered to vary weakly with wavelength; Brown carbon (BrC), a mixture of organic compounds with the ability to absorb light in the ultraviolet (UV) and visible (VIS) regions; and MD, having also a stronger absorption towards short wavelengths. It is known that BC has the highest light absorption efficiency and is the dominant contributor to the absorption process (Kirchstetter et al., 2004; Costabile et al., 2013). However, it has been shown that sometimes the contribution from BrC (Zhu et al., 2017; Yang et al., 2009) and MD (Collaud Coen et al., 2004; Fialho et al., 2005; Wu et al., 2018) cannot be considered negligible. Some studies assume that the influence of either BrC or MD is low and could be roughly neglected. For example, Shu-Zhu et al. (2017) examined the contribution from BrC and BC, while Fialho et al. (2014) only considered the effect of BC and MD. Another option is to distinguish between BC and Non-BC absorbers (a term that includes BrC and/or MD) (Ran et al., 2016; Nicolás et al., 2018). Based on wavelength-dependence and particle size distribution, Yang et al. (2009) attributed aerosol light absorption to BC, BrC and MD, showing that the contribution from non-BC absorbers (NBC), especially BrC, is not negligible at shorter wavelengths.

This work is focused on estimating the contribution from BC, BrC and MD to light absorption at a mountain environment located in the southeast of the Iberian Peninsula. It is important to note that significant contributions from OC and MD to PM levels have been found in the study area (Galindo et al., 2017; Nicolás et al., 2018). In order to facilitate the attribution of light absorption to BC and NBC, this analysis was conducted on periods characterized by high concentrations of MD. Nevertheless, the method used to carry out the apportionment can be applied to the entire study period. The identification of time intervals dominated by specific types of aerosols was performed by means of cluster analysis using some optical properties as variables. PM chemical analyses were used to complement the information obtained from optical parameters. The time resolution used for optical and chemical data was 1 hour. High-time resolution measurements can provide a more comprehensive view of the influence of specific atmospheric processes on the variability of PM. The results obtained can be useful to improve future climate projections performed in the Mediterranean region.

2. Methodology

2.1. Site description

The sampling was carried out for thirteen days at the end of the summer 2014 at a mountain station located in the Aitana peak (38°39 N; 0°16 W; 1558 m a.s.l). The observatory is within a military area (EVA n°5) and is part of the ACTRIS-2 Research Infraestructure as associated partner. The sampling point, located in the southeast of the Iberian Peninsula, is close to the Mediterranean coast and frequently influenced by Saharan dust outbreaks (Fig. 1). The intensity and frequency of these episodes are higher during the summer (Nicolás et al., 2018).

Previous studies related to the chemical composition and optical properties of aerosols at this site can be found in Galindo et al. (2016, 2017), Castañer et al. (2017), and Nicolás et al. (2018, 2019). The meteorological characterization of the study area, together with photographs of the measurement station, can be seen in Galindo et al. (2016).

2.2. Equipment, measurements and data treatment

The study was conducted on an hourly basis, with a total of 307 records obtained during the measurement period (from 00:00 h of 12th September to 18:00 h of 24th September). One-hour averages were calculated from data provided by optical instruments (5-min time resolution) and by an optical particle counter (10-min time resolution).

2.2.1. Scattering and absorption properties

The measurements of σ_{sp} (scattering coeficient) an σ_{bsp} (hemispheric backscattering coeficient) included in this work were obtained from a nephelometer (model Aurora 3000, ECOTECH Pty Ltd., Knoxfield, Australia). This nephelometer provides measurements of σ_{sp} and σ_{bsp} at three wavelengths (450, 525 and 635 nm). The σ_{sp} and σ_{bsp} data were corrected for truncation errors and for non-Lambertian errors using the method described by Müller et al. (2011). A PM_{10} cut-off inlet was used as a sample head in the nephelometer, which is also provided with a processor-controlled automatic heater to assure that measurements were performed under dry conditions (RH < 40%) following GAW (WMO/GAW, 2016) and ACTRIS (www.actris.eu) recommendations. The percentage of valid data was 87%.

In addition, an intensive parameter was obtained from σ_{sp} and σ_{bsp}: Scattering Angstrom Exponent (SAE): SAE hourly values were derived from the following expression:

$$SAE = -\frac{ln\frac{\sigma_{sp}(\lambda_1)}{\sigma_{sp}(\lambda_2)}}{ln\frac{\lambda_1}{\lambda_2}} \quad (1)$$

Where $\lambda_1 = 450$ nm and $\lambda_2 = 635$ nm.

The measurements of σ_{ap} (absorption coeficient) were obtained using an Aethalometer (model AE31, Magee Scientific, USA). The Aethalometer provides the absorption coefficient at seven wavelengths (370, 470, 520, 590, 660, 880 and 950 nm; Hansen et al., 1984). To obtain the aerosol absorption coefficient from the aerosol attenuation coefficient, corrections using the procedure developed by Weingartner et al. (2003) were applied to compensate the filter-loading effects. To compensate the multi-scattering effects due to the filter fibres, we used a C factor of 3.5 (with an uncertainty of 25%) following the recommendations given by Muller (2015) (ACTRIS-2 WP3 Workshop). The instrument operates with a constant air flow rate of 3.9 L m^{-1} with no cut-off inlet in total suspended particle mode. In order to avoid noise problems that may affect the spectral dependence of the absorption coefficient, we used the criterion proposed by Rizzo et al. (2011), which is based on adjusting each spectral measurement to a quadratic fit and rejecting those whose coefficient of determination is less than 0.85. With the application of this criterion, the percentage of valid data was 83%.

An intensive parameter was obtained from σ_{ap}: Absorption Angstrom Exponent (AAE): AAE hourly values were derived from the following expression:

$$AAE = -\frac{ln\frac{\sigma_{ap}(\lambda_1)}{\sigma_{ap}(\lambda_2)}}{ln\frac{\lambda_1}{\lambda_2}} \quad (2)$$

Where $\lambda_1 = 370$ nm and $\lambda_2 = 950$ nm.

Values of SSA (Single Scattering Albedo) were also derived from σ_{ap} and σ_{sp}:

$$SSA = \frac{\sigma_{sp}}{\sigma_{sp} + \sigma_{ap}} \quad (3)$$

SAE, AAE and SSA values are wavelength dependent. Summary tables showing aerosol optical property thresholds used to determine the predominant aerosol type can be found in Schmeisser et al. (2017) and Valentini et al. (2020). Generally, SAE < 1 refers to coarse mode aerosols, while SAE > 2 indicates a large contribution from fine mode aerosols (Schuster et al., 2006). When the dominant component is MD, negative values also occur (Collaud Coen et al., 2004). Negative values are also assigned to marine particles (Seinfeld and Pandis, 2016). If BC is the dominant absorbing aerosol component, the AAE value is close to 1 (Bergstrom et al., 2007). Alternatively, AAE values for BrC and MD are higher than 1 (Kirchstetter et al., 2004). An SSA value of 0.85 is often used as a threshold to differentiate between a low and a high absorption. SSA values close to 1 indicate the presence of low or non-absorbing

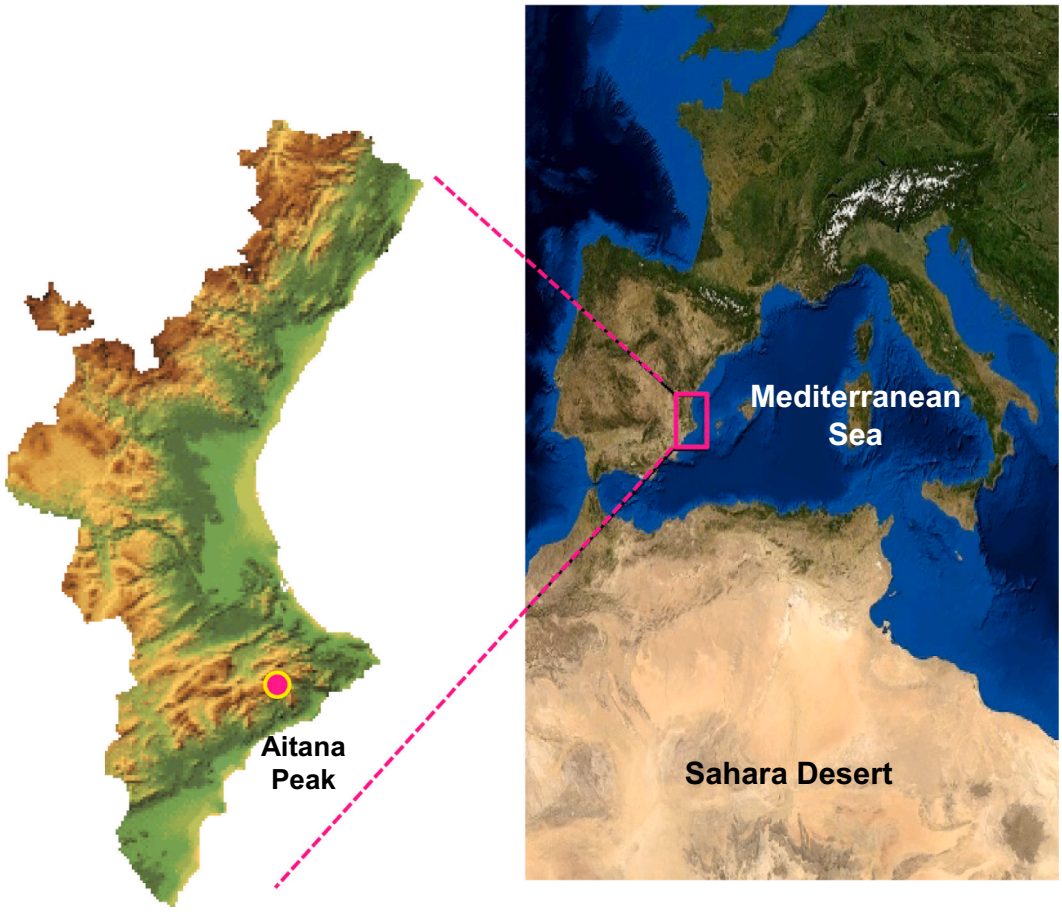

Fig. 1. Location of the sampling site in the southeast of the Iberian Peninsula.

aerosols, while values below 0.85 indicate the presence high absorbing aerosols (Schmeisser et al., 2017).

2.2.2. PM and chemical composition

Samples of fine ($PM_{2.5}$) and coarse ($PM_{10-2.5}$) particulate matter were collected with 1-h time resolution using a "Streaker" sampler (PIXE International Corporation-http://pixeintl.com/Streaker.asp). A detailed description of this sampler can be found in Prati et al. (2000) and Lucarelli et al. (2000). The elemental composition for both fractions was obtained by the PIXE (Particle-Induced X-ray Emission) technique. PIXE analyses were performed with 3 MeV protons from the 3 MV Tandetron accelerator of the LABEC laboratory of INFN in Florence, with the external beam set-up extensively described elsewhere (Calzolai et al., 2010; Lucarelli, 2020; Lucarelli et al., 2018). The percentage of valid samples for both fractions was higher than 70% for most elements (Na, Mg, Al, Si, S, Cl, K, Ca, Cr, Mn, Fe, Ni, Cu, Zn, Br). Elements with less than 30% of valid data were not considered.

To determine the hourly concentration of MD in the fine fraction (Fine-MD), the following equation was used (Chow et al., 2015):

$$MD = 2.2 \cdot Al + 2.49 \cdot Si + 1.63 \cdot Ca + 1.49 \cdot Ti + 2.42 \cdot Fe \quad (4)$$

It should be noted that OC daily concentrations in the PM_{10} fraction during the sampling period were take from the work conducted by Galindo et al. (2017) at the same measurement station. OC concentrations varied little throughout the study period, with a mean value of 1.9 μg m^{-3} and a standard deviation of 0.4 μg m^{-3}. This additional information is useful since BrC consists of a wide variety of organic compounds (Yang et al., 2009).

On the other hand, PM_{10} and $PM_{2.5}$ hourly concentrations were measured by a GRIMM 190 optical counter. The concentrations of both size fractions were used to: a) understand the temporal variability of the optical parameters; b) obtain MAE (Mass Absorption Efficiency) and MSE (Mass Scattering Efficiency) values, and c) identify the meteorological events occurring during the sampling period.

2.2.3. Cluster analysis

Cluster analysis (CA) is a multivariate statistical technique used for grouping elements (or variables) into different categories or clusters with maximum homogeneity within themselves and maximum heterogeneity between them. In this study the non-hierarchical K-means method was used in order to classify different groups representing time periods characterized by aerosols with similar chemical composition, concentration and size. The variables (as hourly averages) used to discriminate between different types of aerosols were: SAE (as an indicator of particle size), AAE (providing information about aerosol chemical composition) and $\log(\sigma_{sp})$. The logarithm of scattering coefficient represents the aerosol loading. We decided to use $\log(\sigma_{sp})$ instead of the σ_{sp} value so that the values of the three variables are more comparable and hence the clustering is not dominated by σ_{sp} (Schmeisser et al., 2017). The 3D clustering has been used in several previous studies (Omar et al., 2005; Szkop et al., 2016; Schmeisser et al., 2017) with good results. A total of 4 clusters representing four discontinous time periods characterized by similar SAE, AAE and $\log(\sigma_{sp})$ values were selected.

3. Results

3.1. PM and optical properties

Table 1 shows different statistical parameters of PM and optical properties obtained during the measurement period. Regarding PM concentrations, mean values for both mass fractions were similar, although the standard deviation (SD) for coarse particles was much higher. The higher variability of $PM_{10–2.5}$ levels may be due to its greater sensitivity to different meteorological episodes such as Saharan dust outbreaks or rainfall events (Nicolás et al., 2020).

The comparison between the aerosol optical properties shown in Table 1 and reference values obtained in other works conducted at regional background sites should be carried out with caution since the monitoring periods are different. In addition, it must be considered that the present study was performed at the end of the summer, when extensive optical parameters and PM levels at the study area are highest (Castañer et al., 2017; Nicolás et al., 2018).

Mean values of scattering parameters were within the ranges obtained at different European mountain stations (Pandolfi et al., 2018). Although measurements were carried out in late summer, σ_{sp} and σ_{bsp} average values were similar to those recorded in autumn at the same sampling point (Castañer et al., 2017). On the other hand, the σ_{sp} median value indicates that SDE marginally affected the mean value of the scattering coefficient.

Scattering processes were dominated by coarse particles, as indicated by the mean SAE value (0.87). This is an unusual value for a remote station since SAE values are frequently above 1.50 in this type of location. However, the SAE value obtained in this study was very close to that recorded at the Izaña station in the Canary Islands (2373 m a.s.l) due to the significant contribution of coarse particulate matter at this site as a consequence of its proximity to North Africa. (Andrews et al., 2011; Pandolfi et al., 2018).

The median value of σ_{ap} (525 nm) was in the upper range of values recorded at mountain environments (Andrews et al., 2011). On the other hand, the average value of AAE (1.24) suggests a limited contribution from non-BC absorbing components to the absorption process. Typically for mountain environments, the SSA mean value (0.88) indicates a predominance of scattering aerosols compared to absorbing aerosols.

MSE and MAE mean values were, respectively, 3.20 ± 0.14 m^2 g^{-1} ($R^2 = 0.65$) and 0.38 ± 0.02 m^2 g^{-1} ($R^2 = 0.62$) for the fine fraction. The R^2 values for the coarse fraction were significantly lower.

3.2. Identification of time periods using cluster analysis

3.2.1. Characteristics of clusters

The cluster technique (K-means) was applied to hourly data with the aim of obtaining different time periods characterized by homogeneous values of aerosol optical properties. To obtain the clusters, as mentioned in Section 2.2.3, three variables were used: AAE, SAE and $\log(\sigma_{sp})$ (Mm^{-1}) for $\lambda = 525$ nm. As shown in Fig. 2, four different clusters (C) were obtained.

At first sight, some differences among the four clusters can be observed. The greatest differences were between clusters C1 and C4, while clusters C3 and C2 were more similar. To properly identify the differences between them, Table 2 shows mean values of PM concentrations and optical properties for each group. The percentage of data (number of hours) for each cluster is also indicated.

C1 presented the highest $PM_{2.5}/PM_{10}$ and SAE values and the lowest values of σ_{ap}, σ_{sp}, PM, BC and SSA. These outcomes indicate that C1 was dominated by fine particles. This cluster corresponded to the cleanest air, since $PM_{2.5}$ and $PM_{10–2.5}$ concentrations were below 5 and 3 μg m^{-3}, respectively. C1 included only 10.4% of the data.

C4 included 15% of the data and showed opposite features to C1. C4 was characterized by the presence of coarse particles (SAE = −0.59) and had the highest values of $PM_{10–2.5}$, $PM_{2.5}$ and σ_{sp}. C4 also registered the highest AAE value (1.58), indicating that the NBC contribution to light absorption was highest for this cluster. Although C4 showed the maximum SSA value, the σ_{ap} value was not as high as expected. The analysis of this result will be carried out in Section 3.4.1.

Clusters 2 and 3 exhibited intermediate values between those of C1 and C4 for most of the measured variables. In spite of this, C3 presented the highest σ_{ap} value. The SAE value was quite different between both clusters. Coarse particles had a greater influence on the scattering process for C2. Almost 75% of the data were included in clusters 2 and 3.

Table 1
Summary statistics of BC, aerosol optical properties and PM concentrations over the measurement period.

	Mean	SD	Min	P5	Median	P95	Max
$\sigma_{sp,520\ nm}$	19.3	11.1	0.8	4.7	17.7	39.1	68.4
$\sigma_{bsp,520\ nm}$	2.9	1.4	0.4	0.9	2.6	5.8	7.7
$\sigma_{ap,525\ nm}$	2.5	1.2	0.3	0.9	2.5	4.5	6.1
SAE $_{(450–635\ nm)}$	0.87	0.84	−1.33	−0.67	0.96	2.16	4.44
AAE $_{(370–950\ nm)}$	1.24	0.32	0.71	0.82	1.21	1.77	2.31
SSA $_{(520\ nm)}$	0.88	0.08	0.42	0.73	0.88	0.95	0.98
BC	254.1	125.7	20.0	76.6	241.6	457.0	678.3
$PM_{2.5}$	6.1	2.8	0.9	2.2	6.0	10.6	14.0
$PM_{10–2.5}$	6.5	5.6	0.9	1.6	4.4	17.5	32.4

Min: Minimum; Max: Maximum; P5: 5th Percentil; P95: 95th Percentil.
σ_{sp}, σ_{bsp}, σ_{ap} are given in Mm^{-1}, BC in ng m^{-3} and PM concentrations in μg m^{-3}.
AAE, SAE and SSA are dimensionless.

3.2.2. Temporal evolution

Fig. 3 presents the temporal evolution of PM mass concentrations and some optical properties. The time periods included in each cluster are shown in Fig. 3a.

Fig. 3b depicts the temporal evolution of coarse PM concentrations and the $PM_{2.5}/PM_{2.5–10}$ ratio. Rainfall events are also indicated. $PM_{2.5–10}$ concentrations increased significantly during two periods. The first one was from the evening of 16 September to the early morning of 17 September, while the second one was from 20 to 22 September. During the morning of 22 September the highest $PM_{2.5–10}$ concentration (~30 μg m^{-3}) and the minimum $PM_{2.5}/PM_{2.5–10}$ ratio (~0.3) were recorded. At the end of the measurement period a precipitation event occurred, with rainfall rates greater than 5 L m^{-2}. Simultaneosly, the $PM_{2.5}/PM_{2.5–10}$ ratio reached values above 0.7. The two periods characterized by increases in the concentrations of coarse particles were identified as Saharan dust events (SDE), named SDE1 and SDE2, respectively. The identification of SDE was performed by means of forecast models (BSC/DREAM8b and NAAPS). Both events had a low impact on PM levels compared with other SDE occurring at the sampling site throughout 2014 (Galindo et al., 2017).

The temporal evolution of SAE and AAE can be seen in Fig. 3c. During SDE, SAE values were lowest, while AAE levels were high. The anticorrelation between SAE and AAE is characteristic of dust events, indicating an increased predominance of coarse particles with enhanced absorption at UV wavelengths (Titos et al., 2017).

The variability of σ_{sp} and σ_{ap} is shown in Fig. 3d. The daily evolution of both parameters from the beginning of the sampling period until SDE1 was characterized by a maximum value at midday. This trend is typical of mountain environments (Pandolfi et al., 2011). σ_{sp} and σ_{ap} were maxima during SDE2 (60 Mm^{-1} and 6 Mm^{-1}, respectively), but curiously, while the highest σ_{ap} value was recorded at the beginning of the event, the maximum σ_{sp} value was reached at the end. This outcome will be analyzed in Section 3.4.1. The values of σ_{sp} and σ_{ap} decreased at the onset of the rain.

From Fig. 3, the hourly periods in C4 influenced by Saharan dust can be identifed with a fair degree of certainty. On the other hand, the SSA value obtained for this cluster was quite high (0.93) (see Table 2), as usually observed in the Iberian Peninsula during Saharan dust events

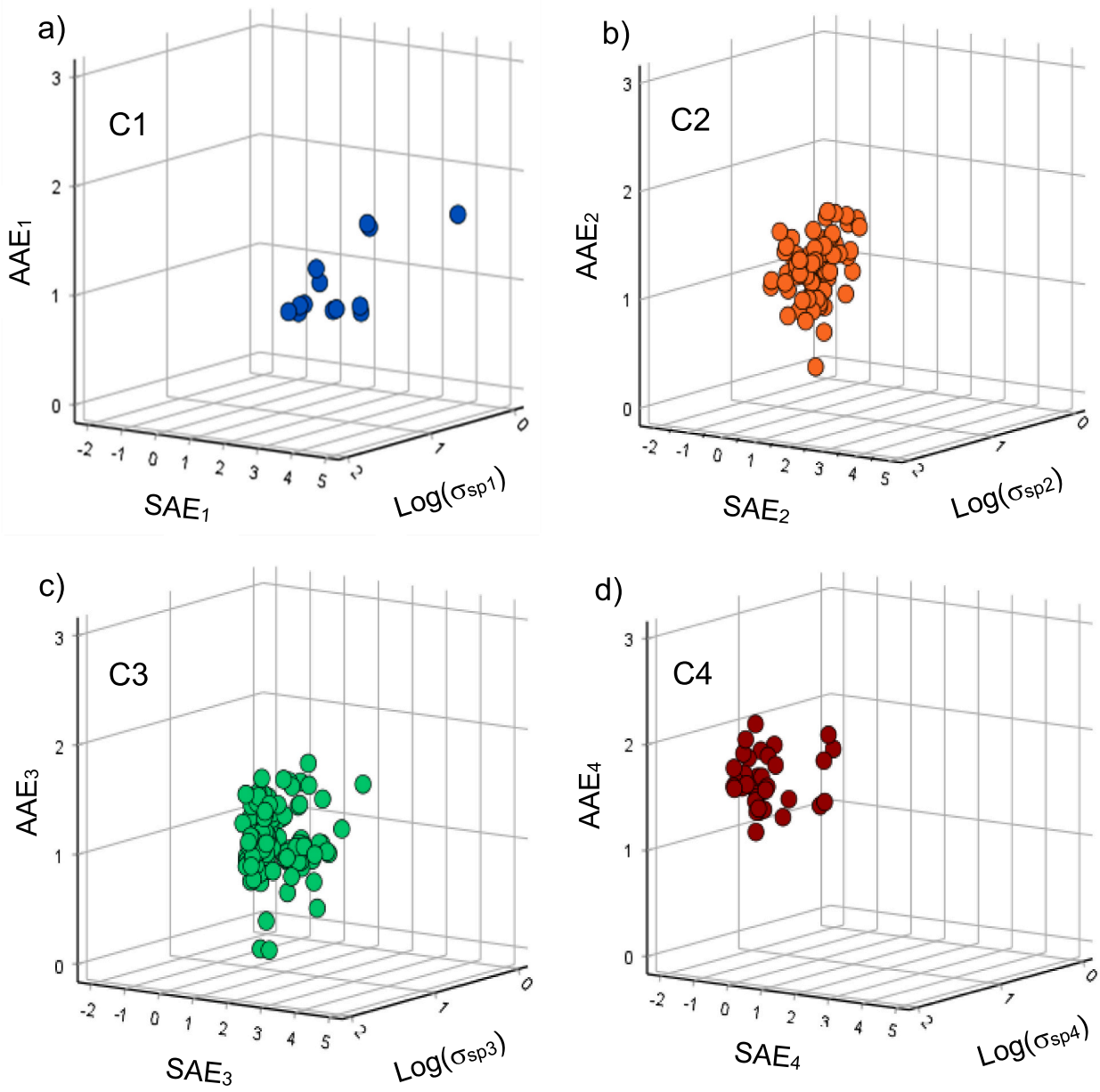

Fig. 2. Three-dimensional parameter spaces of SAE, AAE and log(σ_{sp}) resulting from cluster analysis.

Table 2
Mean values (standard deviation) of optical properties and PM concentrations for each cluster.

Parameter	C1	C2	C3	C4
N (%)	32 (10.4)	95 (30.9)	134 (43.6)	46 (15)
$\sigma_{sp,520\ nm}$	10.6 (7.7)	17.5 (8.6)	19.4 (9.3)	29.2 (16.2)
$\sigma_{ap,525\ nm}$	2.0 (0.9)	2.5 (1.0)	2.8 (1.3)	2.2 (0.9)
SAE $_{(450–635\ nm)}$	2.89 (0.60)	0.55 (0.26)	1.29 (0.28)	−0.59 (0.30)
AAE $_{(370–950\ nm)}$	1.20 (0.37)	1.23 (0.24)	1.16 (0.29)	1.58 (0.29)
SSA $_{(520\ nm)}$	0.84 (0.10)	0.88 (0.07)	0.87 (0.11)	0.93 (0.08)
BC	165.1 (88.7)	261.5 (97.4)	287.3 (145.5)	207.7 (90.9)
$PM_{2.5}$	4.3 (2.0)	5.7 (2.2)	6.2 (2.8)	7.9 (3.3)
$PM_{10–2.5}$	2.8 (1.4)	6.1 (4.5)	5.4 (3.3)	13.3 (8.7)
$PM_{2.5}/PM_{10}$	0.61 (0.17)	0.48 (0.12)	0.55 (0.12)	0.37 (0.10)

σ_{sp}, σ_{ap} are given in Mm^{-1}, BC in ng m^{-3} and PM concentrations in μg m^{-3}. AAE, SAE, SSA and $PM_{2.5}/PM_{10}$ are dimensionless.

(>0.9) (Cachorro et al., 2008; Valenzuela et al., 2012; Gómez-Amo et al., 2017; Titos et al., 2017). C1 occured mainly at the end of the sampling period, when rainfall started. The first four days of the study period were dominated by C3. During this period, σ_{sp} and σ_{ap} values showed the typical daily evolution expected for regional or mountain environments on non-event days. Considering the mean SAE value obtained for C3 (1.29), it is difficult to clearly identify a dominant type of aerosol, and therefore it must be considered as a mixed aerosol case (Gómez-Amo et al., 2017). Most of the hourly periods between the two SDE, including those at the begining of SDE2, were included in C2. As seen in Table 2, PM levels and optical properties in C2 were very similar to those of C3. However, the SAE mean value for C2 was quite lower. This was probably because MD was resuspended in the atmophere the days after SDE1.

3.3. Chemical characterization of the clusters

Table 3 shows mean concentrations of the elements analyzed in both size fractions during the measurement period. Only elements with more

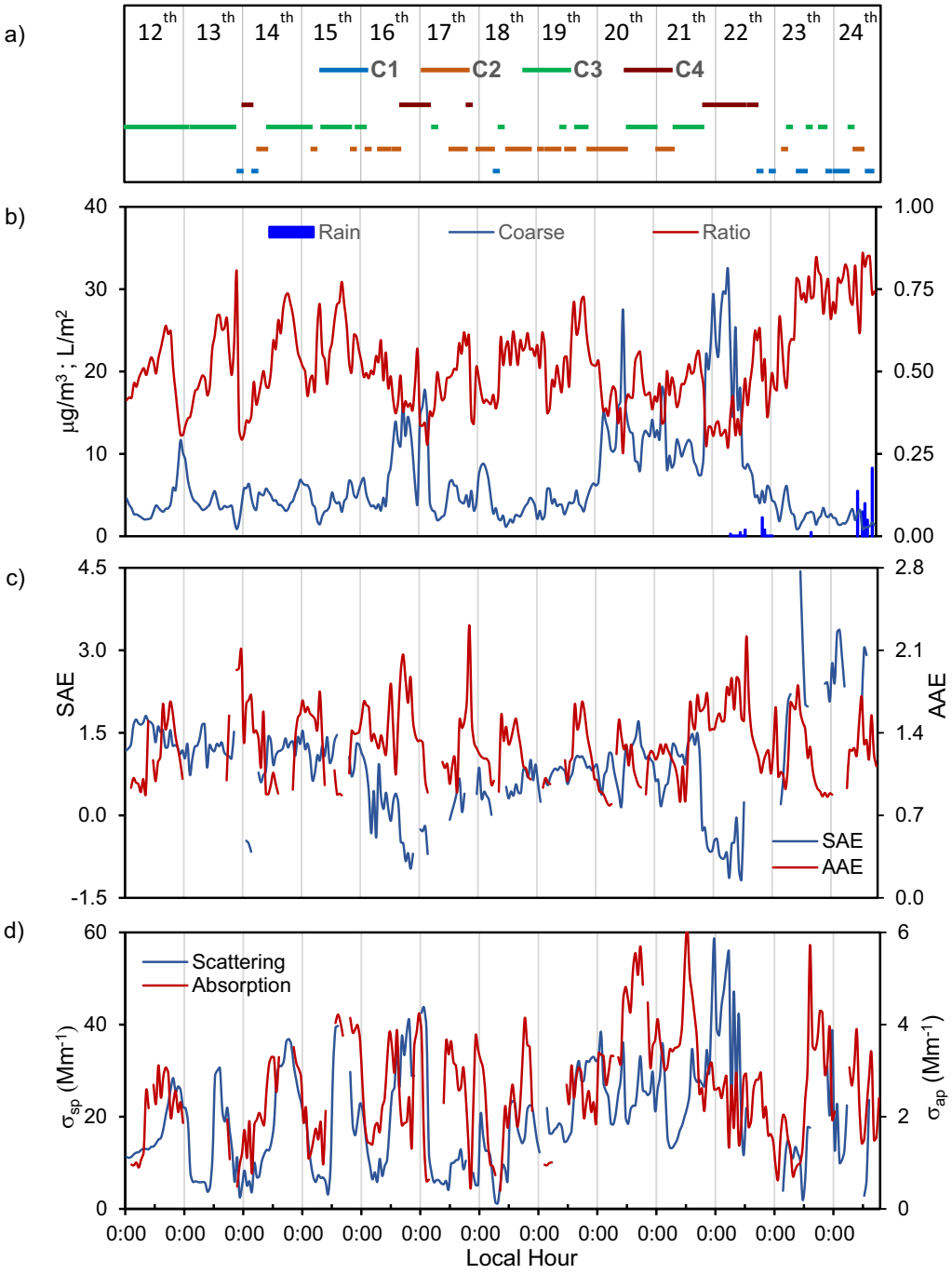

Fig. 3. a) Allocation of hourly periods to the k clusters. Temporal evolution of: b) coarse PM (in μg m^{-3}), $PM_{2.5}/PM_{10}$ ratio and rain (L m^{-2}), c) SAE and AAE, d) σ_{sp} and σ_{ap} (in Mm^{-1}).

than 70% of valid measurements are included in this table.

Crustal (Si, Al, Ca, Fe) and marine (Na, Cl) elements showed the highest concentrations in the coarse fraction, as expected from the location of the sampling point. Sulfur was the most abundant element in the fine fraction, followed by crustal elements. Regarding mass size distributions, marine and crustal elements were found mainly in the coarse fraction, while S was distributed primarily in the fine fraction. Elements such as Cu and Zn were almost evenly distributed between the two fractions.

As can be observed in Table 3, mean concentrations of crustal elements, such as Al, Si, Ca, Ti and Fe, were considerably higher than median values in both fractions. This suggests that these elements are very sensitive to short-term episodes.

Fig. 4 illustrates the variation of the mean concentration (C) of each element as a function of the cluster for both mass fractions. The impact factor (IF_{ijc}) for each element (i), in each mass fraction (j) and cluster (c) was determined as follows:

$$IF_{ijc} = \frac{\langle C_{ijc} \rangle}{\langle \overline{C_{ij}} \rangle} \quad (5)$$

Where $\langle \overline{C_{ij}} \rangle$ is the average concentration of the element "i" in the mass fraction "j" shown in Table 3.

IF values for most elements showed the greatest variations in C1 and C4. IFs for almost all elements were less than 1 in the first cluster, especially in the coarse fraction. This outcome indicates that coarse particles are removed more efficiently by wet scavenging than fine particles. An opposite behaviour was observed for C4. Except for marine elements, an overall increase in IF values was observed in the coarse fraction. In contrats, in the fine fraction, only crustal elements showed IF values higher than 3. Therefore, it can be stated that significant contributions from MD to $PM_{2.5}$ during SDEs occurred. C2 showed IF values close to 1 for both size fractions, indicating that time periods included in C2 were not affected by meteorological events. Almost half of the hourly periods were included in C3. Therefore, it should be noticed that the mean values shown in Table 3 were highly influenced by the levels recorded for this cluster. IF values in C3 were quite similar to those in C2. Nevertheless, a significant decrease in IF values for crustal elements were observed in both fractions, with values lower than 0.5 in $PM_{2.5}$.

3.4. Contribution of non-BC absorbing components to σ_{ap}

3.4.1. Analysis of the absorption process in C4

As already mentioned, the highest mean AAE value (1.58) was obtained for C4; however, the mean value of $\sigma_{ap,520nm}$ (2.2 Mm^{-1}) was not as high as expected. As can be observed in Fig. 3, during the first half of 22 September the maximum concentration of particles was reached, which was due to SDE2. During the same period of the day, AAE values were higher than 2.00. However, σ_{ap} values decreased significantly with respect to those registered the day before.

When MAE values were calculated for each cluster separately (Fig. 5), the value obtained for C4 was clearly lower than those for the remaining clusters. MAE values for C1, C2 and C3 were quite similar, but the value obtained during the SDE decreased to 0.26 ± 0.07 $m^2\ g^{-1}$.

This result may explain the low σ_{ap} values for C4, particulary during SDE2. Furthermore, if the temporal evolution of Fine-MD and BC are represented (Fig. 6), a clear decrease in BC concentrations was observed on 22 September, coinciding with the maximum peak in MD levels.

Since MD is less efficient in absorbing light than BC, the MAE value for C4 was lower than for the remaining clusters.

3.4.2. Methodology to differentiate non-BC absorbing components

Data included in C4 were used to obtain the contribution to light absorption from BC, MD and BrC. C4 was selected because the proportion of MD was highest in this cluster, leading to a better apportionment. In spite of this, the procedure described in this section could be performed for the whole period.

As a preliminary step, the contribution of NBC was determined. Fig. 7a presents the average spectral dependence of σ_{ap} for the whole period. To determine the contribution from NBC to light absorption, it was assumed that pure BC is the only absorbing component at $\lambda = 950$ nm and that its spectral dependence for the remaining wavelengths is a function of λ^{-1}. The contribution from NBC for each wavelength was estimated from the differences between measured σ_{ap} values and those calculated as a function of $\sim\lambda^{-1}$. This methodology based on spectral differences has been used in several previous studies with the objective of determining the contribution from NBC to light absorption (Ran et al., 2016; Shen et al., 2017; Nicolás et al., 2018).

As can be observed, the contribution from NBC was highest in the UV/near-VIS region. Fig. 7b shows the mean relative contribution from NBC to total light absorption between 370 nm and 950 nm. The figure

Table 3
Mean elemental concentrations in ng m^{-3} for the coarse and fine fractions.

	Coarse					Fine				
	Mean	SD	Median	P5	P95	Mean	SD	Median	P5	P95
Na	351.5	217.8	318.1	74.5	738.4	62.2	27.6	61.0	24.2	110.4
Mg	147.8	104.8	119.8	41.2	346.7	33.1	29.1	23.7	13.7	99.6
Al	450.8	475.0	269.3	81.8	1448.1	111.6	169.2	45.0	11.8	524.5
Si	1047.1	1101.7	628.7	167.7	3275.3	246.7	368.7	109.6	24.2	1169.9
P	9.9	6.1	7.8	3.6	23.1	29.4	11.2	28.5	20.8	37.3
S	75.7	38.6	67.6	25.8	150.5	328.3	177.5	269.4	123.6	641.6
Cl	201.6	190.9	136.4	22.0	590.1	18.5	4.6	17.9	12.5	27.3
K	157.6	134.3	104.9	40.5	438.4	73.1	44.0	64.0	23.7	160.5
Ca	693.1	555.2	538.5	117.5	1885.5	70.7	97.5	41.2	18.9	209.2
Ti	25.9	26.8	15.0	4.7	84.9	12.1	12.6	6.3	3.3	44.9
Cr	1.9	1.0	1.7	1.0	3.7	2.9	1.0	2.8	1.4	4.7
Mn	5.0	4.6	3.2	1.2	14.2	2.1	1.7	1.5	0.9	5.9
Fe	264.2	263.1	164.9	50.2	816.2	67.3	99.6	27.8	10.9	317.0
Ni	0.5	0.2	0.5	0.2	0.9	1.0	0.6	0.9	0.5	2.3
Cu	0.8	0.6	0.7	0.2	1.9	0.6	0.2	0.6	0.4	0.9
Zn	2.0	2.3	1.6	0.6	3.6	1.7	0.8	1.7	0.6	3.3
Br	0.7	0.4	0.6	0.3	1.5	1.5	0.5	1.5	0.7	2.3
Rb	1.0	1.0	0.7	0.3	3.2	–	–	–	–	–
Sr	2.5	1.6	2.2	0.6	5.9	–	–	–	–	–
Ba	22.8	16.9	15.3	6.8	56.4	–	–	–	–	–
Pb	1.1	0.6	0.9	0.4	2.1	2.3	1.2	1.9	0.9	4.8

Standard Deviations (SD), Median and 95th and 5th percentiles (P95, P5) are also shown.

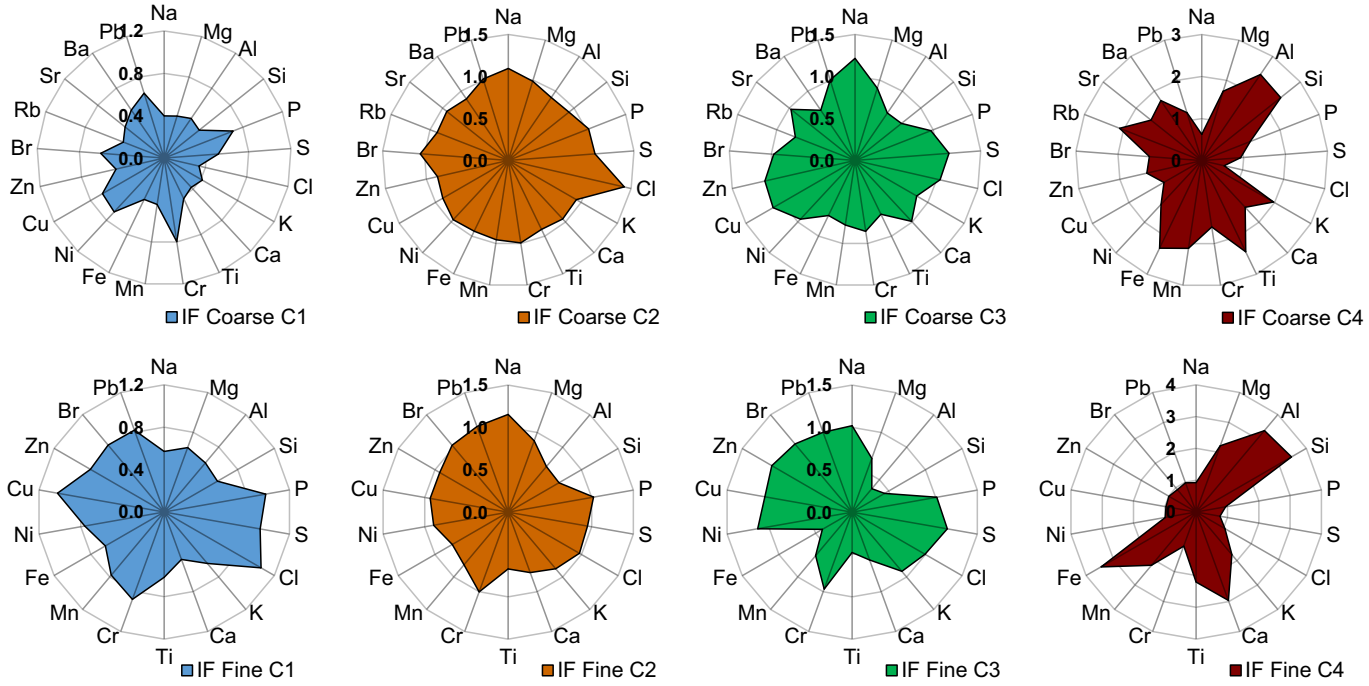

Fig. 4. Impact factors (IF) for each element in the fine and coarse fractions for each cluster.

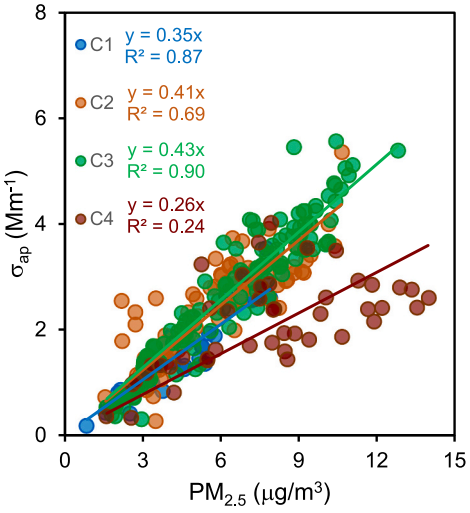

Fig. 5. Correlations between absorption coefficients (σ_{ap} in Mm^{-1} at 525 nm) and $PM_{2.5}$ concentrations (μg m^{-3}) for the four clusters. The linear fits are also shown.

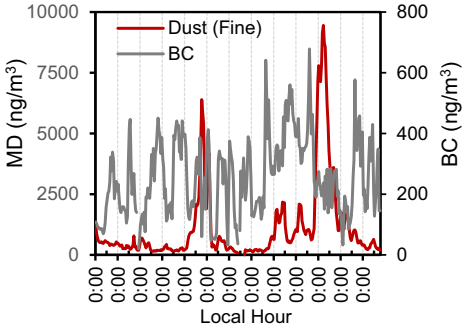

Fig. 6. Temporal evolution of BC (ng m^{-3}) and Fine-MD (ng m^{-3}) concentrations.

also shows the percentage contribution corresponding to C4. This contribution was between twice and three times the mean values for the short wavelengths. The percentage reached 40% in the UV range for this cluster.

To discriminate the contributions from BrC and MD in C4, the σ_{ap} value for NBC (σ_{ap}-NBC, $\lambda = 520$ nm) was represented versus the concentration of Fine-MD (Fig. 8). The values of σ_{ap}-NBC were obtained using the methodology based on spectral differences described above.

In order to separate the contributions from MD (σ_{Dust}) and BrC (σ_{BrC}), it was considered that a high coefficient of determination (R^2) between Fine-MD concentrations and σ_{ap}-NBC implied that the absorption was mostly due to MD. On this basis, the approach consisted of drawing a line including points aligned in the lower end of the chart. The equation of this line can be used to estimate σ_{Dust}. As can be seen in Fig. 8a, a high determination coefficient ($R^2 = 0.91$) was obtained. The slope (0.032 ± 0.004 m^2 g^{-1}) represented the MAE value for Fine-MD at 520 nm. As indicated in the figure, absorption coefficients falling above the regression line had contributions from both MD and BrC. The procedure used for the determination of σ_{Dust}, σ_{BrC}, σ_{BC} and MAE values for all wavelengths is described in the Supplementary material.

Table 4 shows MAE values for Fine-MD obtained for the remaining wavelengths.

MAE values decreased as the wavelength increased and therefore the absorption due to MD was reduced. MAE values shown in Table 4 are in good aggrement with those obtained for the $PM_{2.5}$ fraction by Caponi et al. (2017) when air masses came from the Sahara Desert (MAE = 0.033–0.037 m^2 g^{-1} for $\lambda = 532$ nm), but they were slightly lower than that obtained by Wu et al. (2018) (MAE = 0.014 m^2 g^{-1} for $\lambda = 637$ nm).

The percentage contribution to light absorption from BC, BrC and MD for C4 is shown in Fig. 8b. The absorption coeficients and the contributions from the different absorbing components to light absorption for the four clusters are presented in the Supplementary Material. As can be seen, although the MD concentration for C4 was quite high (3.9 μg m^3 - mean value), the BrC contribution was slightly higher than that from MD for most wavelengths. For $\lambda = 520$ nm, ~6% of the absorption was due to MD and ~ 8% to BrC. Due to the short study period, it is dificult to

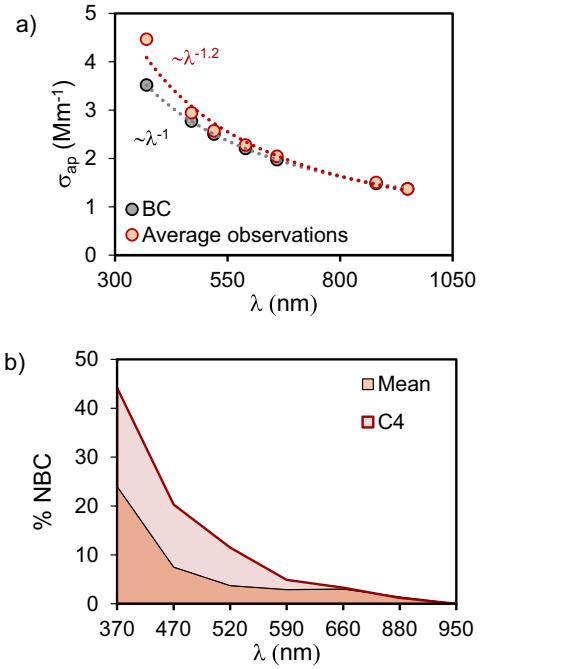

Fig. 7. a) Average σ_{ap} at seven wavelengths (marked as red dots; data were fitted using a power function). The grey dots show the wavelength dependence of σ_{ap} for pure BC. The Angstrom exponents for each fit are shown in the corresponding colors. b) Mean percentage contribution to the light absorption coefficient from NBC. Percentages for cluster C4 are also shown. (For interpretation of the references to colour in this figure legend, the reader is referred to the web version of this article.)

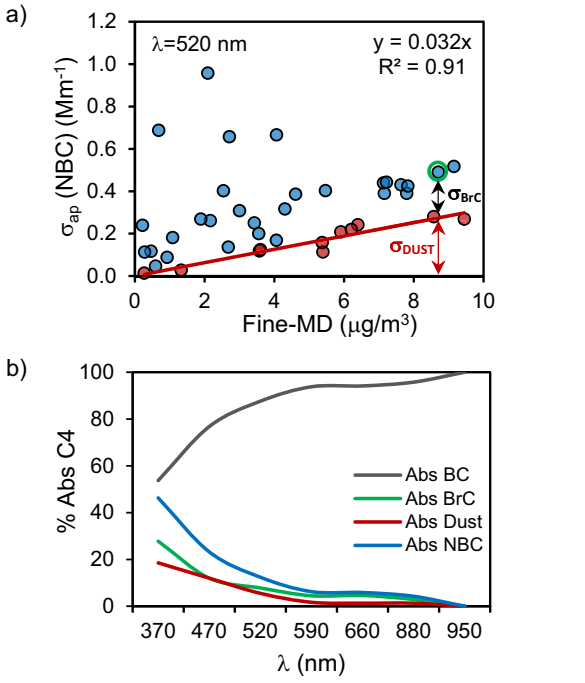

Fig. 8. a) Scatter plot of σ_{ap} (NBC) versus Fine-MD concentrations. The red line was drawn including points aligned in the lower end of the chart and represents values of σ_{ap} associated with MD absorption. The equation of this line can be used to estimate σ_{Dust}. b) Relative contribution from BC, BrC and MD to the total light absorption for cluster C4. (For interpretation of the references to colour in this figure legend, the reader is referred to the web version of this article.)

Table 4
MAE values for Fine-MD at UV and VIS wavelengths for C4.

λ (nm)	R^2	MAE ± Error (m^2 g^{-1})
370	0.96	0.226 ± 0.030
470	0.91	0.075 ± 0.010
520	0.91	0.032 ± 0.004
590	0.80	0.007 ± 0.002
660	0.61	0.005 ± 0.003

compare the results obtained in this work with those of other similar studies. In the Tibetan Plateau (3300 m a.s.l), Zhao et al. (2019) calculated the percentage contribution of dust to light absorption using MAE_{DUST} values from Caponi et al. (2017). An annual average contribution of 8.5% at 405 nm was obtained. This percentage was significantly lower than that calculated here for C4 (18.5%; λ = 370 nm). Nevertheless, it was higher than that obtained for the remaining clusters, since MD concentrations were much lower for these clusters. For instance, the contribution of MD to light absorption at 370 nm was only 3.6% for C2. In fact, the percentage contributions of dust to light absorption at middle visible wavelengths was less than 1% for C1, C2 and C3 (see Supplementary Material). It is assumed that for these clusters light absorption from non-BC components was mainly due to BrC.

Considering that the OC concentration was quite stable during the whole study period, it can be stated that the contribution from BrC to the absorption process was higher than that from MD.

4. Conclusions

Three optical parameters were used as input variables in Cluster analysis in order to identifiy up to four time periods characterized by different types of aerosols. The differentiation was verified from the aerosol chemical composition. One of the clusters (C4) was clearly associated with high mineral dust loadings. This identification was based on the high values of σ_{sp} (29.2 Mm^{-1}), $PM_{2.5}$ (7.9 μg m^{-3}) and AAE (1.58), and the low SAE value (−0.58) obtained for that cluster. In addition, the chemical analysis of the samples belonging to C4 (with IF values >2 for crustal elements) supports that MD was the dominant type of aerosol. This period, characterized by high Fine-MD concentrations, was used to propose a methodology in which PM chemical composition and optical parameters were combined with the aim of discriminating the contribution from BC, BrC and MD to the light absorption process. The absorption from BrC and MD at short wavelengths was similar, with a slightly higher contribution from BrC. Therefore, it can be concluded that, when MD is not the dominant type of aerosol, the absorption due to BrC is higher than that from MD. This procedure also provided the MAE value for Fine-MD (0.032 m^2 g^{-1} for λ = 520 nm). This value is in good agreement with those obtained in other similar studies.

Declaration of Competing Interest

The authors declare that they have no known competing financial interests or personal relationships that could have appeared to influence the work reported in this paper.

Acknowledgements

This work was supported by the Spanish Ministry of Science, Innovation and Universities (COSMOS Project, ref. RTI2018-098639-B-I00). A. Clemente thanks the Spanish Ministry of Education for a predoctoral grant (FPU18/00081). A. López-Caravaca thanks the Spanish Ministry of Science and Innovation for a predoctoral grant (PRE2019-089098). The authors would also like to thank ACTRIS-Spain network (CGL2017-90884-REDT).

Appendix A. Supplementary data

Supplementary data to this article can be found online at https://doi.org/10.1016/j.atmosres.2021.106000.

References

Andrews, E., Ogren, J.A., Bonasoni, P., Marinoni, A., Cuevas, E., Rodriguez, S., Sun, J.Y., Jaffe, D.A., Fischer, E.V., Baltenperger, U., Weingartner, E., Coen, M.C., Sharma, S., Macdonald, A.M., Leaitch, W.R., Lin, N.H., Laj, P., Arsov, T., Kalapov, I., Jefferson, A., Sheridan, P., 2011. Climatology of aerosol radiative properties in the free troposphere. Atmos. Res. 102, 365–393. https://doi.org/10.1016/j.atmosres.2011.08.017.

Bergstrom, R.W., Pilewskie, P., Russell, P.B., Redemann, J., Bond, T.C., Quinn, P.K., Sierau, B., 2007. Spectral absorption properties of atmospheric aerosols. Atmos. Chem. Phys. 7, 5937–5943. https://doi.org/10.5194/acp-7-5937-2007.

Cachorro, V.E., Toledano, C., Prats, N., Sorribas, M., Mogo, S., Berjón, A., Torres, B., Rodrigo, R., de la Rosa, J., de Frutos, A.M., 2008. The strongest desert dust intrusion mixed with smoke over the Iberian Peninsula registered with Sun photometry. J. Geophys. Res. 113, D14S04. https://doi.org/10.1029/2007JD009582.

Calzolai, G., Chiari, M., Lucarelli, L., Nava, S., Portarena, S., 2010. Proton induced γ-ray emission yields for the analysis of light elements in aerosol samples in an external beam set-up. Nucl. Instrum. Methods Phys. Res., Sect. B 268, 1540–1545. https://doi.org/10.1016/j.nimb.2010.03.002.

Caponi, L., Formenti, P., Massabó, D., Di Biagio, C., Cazaunau, M., Pangui, E., Chevaillier, S., Landrot, G., Andreae, M.O., Kandler, K., Piketh, S., Saeed, T., Seibert, D., Williams, E., Balkanski, Y., Prati, P., Doussin, J.-F., 2017. Spectral-and size-resolved mass absorption efficiency of mineral dust aerosols in the shortwave spectrum: a simulation chamber study. Atmos. Chem. Phys. 17, 7175–7191. https://doi.org/10.5194/acp-17-7175-2017.

Cappa, C.D., Kolesar, K.R., Zhang, X., Atkinson, D.B., Pekour, M.S., Zaveri, R.A., Zelenyuk, A., Zhang, Q., 2016. Understanding the optical properties of ambient sub- and supermicron particulate matter: results from the CARES 2010 field study in northern California. Atmos. Chem. Phys. 16, 6511–6535. https://doi.org/10.5194/acp-16-6511-2016.

Castañer, R., Nicolás, J.N., Crespo, J., Yubero, E., Galindo, N., Caballero, S., Pastor, C., 2017. Influence of air mass origins on optical properties and PM concentrations measured at a high mountain station located in the southwestern Mediterranean. Atmos. Res. 197, 244–254. https://doi.org/10.1016/j.atmosres.2017.07.013.

Cazorla, A., Bahadur, R., Suski, K., Cahill, J.F., Chand, D., Schimd, B., Ramanathan, V., Prather, K.A., 2013. Relating aerosol absorption due to soot, organic carbón, and dust to emission sources determined from in-situ chemical measurements. Atmos. Chem. Phys. 13, 9337–9350. https://doi.org/10.5194/acp-13-9337-2013.

Chow, J.C., Lowenthal, D.H., Chen, L.W.A., Wang, X., Watson, J.G., 2015. Mass reconstruction methods for $PM_{2.5}$: a review. Air Qual. Atmos. Health 8, 243–263. https://doi.org/10.1007/s11869-015-0338-3.

Collaud Coen, M., Weingartner, E., Schaub, D., Hueglin, C., Corrigan, C., Henning, S., Schwikowski, M., Baltensperger, U., 2004. Saharan dust events at the Jungfraujoch: detection by wavelength dependence of the single scattering albedo and first climatology analysis. Atmos. Chem. Phys. 4, 2465–2480. https://doi.org/10.5194/acp-4-2465-2004.

Costabile, F., Barnaba, F., Angelini, F., Gobbi, G.P., 2013. Identification of key aerosol populations through their size and composition resolved spectral scattering and absorption. Atmos. Chem. Phys. 13, 2455–2470. https://doi.org/10.5194/acp-13-2455-2013.

Fialho, P., Cerqueira, M., Pio, C., Cardoso, J., Nunes, T., Custodio, D., Alves, C., Almeida, S.M., Almeida-Silva, M., Reis, M., Rocha, F., 2014. The application of a multi-wavelength Aethalometer to estimate iron dust and black carbon concentrations in the marine boundary layer of Cape Verde. Atmos. Environ. 97, 137–143. https://doi.org/10.1016/j.atmosenv.2014.08.008.

Fialho, P., Hansen, A.D.A., Honrath, R.E., 2005. Absorption coefficients by aerosols in remote áreas: a new approach to decouple dust and black carbón absorption coefficients using seven-wavelength Aethalometer data. J. Aerosol Sci. 36, 267–282. https://doi.org/10.1016/j.jaerosci.2004.09.004.

Galindo, N., Yubero, E., Nicolás, J.F., Crespo, J., Soler, R., 2016. Chemical characterization of PM_1 at a Regional Background site in Western Mediterranean. Aerosol Air Qual. Res. 16, 530–541. https://doi.org/10.4209/aaqr.2015.05.0302.

Galindo, N., Yubero, E., Nicolás, J.F., Crespo, J., Varea, M., Gil-Moltó, J., 2017. Regional and long-range transport of aerosols at Mt. Aitana, Southeastern Spain. Sci. Total Environ. 584-585, 723–730. https://doi.org/10.1016/j.scitotenv.2017.01.108.

Gómez-Amo, J.L., Estellés, V., Marcos, C., Segura, S., Esteve, A.R., Pedrós, R., Utrillas, M. P., Martinez-Lozano, J.A., 2017. Impact of dust and smoke mixing on column-integrated aerosol properties from observations during a severe wildfire episode over Valencia (Spain). Sci. Total Environ. 599-600, 2121–2134. https://doi.org/10.1016/j.scitotenv.2017.05.041.

Hansen, A.D.A., Rosen, H., Novakov, T., 1984. The Aethalometer—An instrument for the real-time measurement of optical absorption by Aerosol particles. Sci. Total Environ. 36, 191–196. https://doi.org/10.1016/0048-9697(84)90265-1.

Kaskaoutis, D.G., Grivas, G., Stavroulas, I., Liakakou, E., Dumka, U.C., Dimitriou, K., Gerasopoulos, E., Mihalopoulos N, 2021. In situ identification of aerosol types in Athens, Greece, based on long-term optical and on online chemical characterization. Atmos. Environ. 246, 118070. https://doi.org/10.1016/j.atmosenv.2020.118070.

Kirchstetter, T., Novakov, W., Hobbs, P.V., 2004. Evidence that the spectral dependence of light absorption by aerosols is affected by organic carbon. J. Geophys. Res. 109, D221208 https://doi.org/10.1029/2004JD004999.

Lucarelli, F., 2020. How a small accelerator can be useful for interdisciplinary applications: the study of air pollution. Eur. Phys. J. Plus 135, 538. https://doi.org/10.1140/epjp/s13360-020-00516-3.

Lucarelli, F., Mandò, P.A., Nava, S., Valerio, M., Prati, P., Zucchiatti, A., 2000. Elemental composition of urban aerosol collected in Florence, Italy. Environ. Monit. Assess. 65, 165–173. https://doi.org/10.1023/A:1006486208406.

Lucarelli, F., Calzolai, G., Chairi, M., Nava, S., Carraresi, L., 2018. Study of atmospheric aerosols by IBA techniques: the LABEC experience. Nucl. Instrum. Methods Phys. Res., Sect. B 417, 121–127. https://doi.org/10.1016/j.nimb.2017.07.034.

Muller, T., 2015. Development of correction factors for aethalometers AE31 and AE33. In: ACTRIS-2 WP3 Workshop, Athens, 10-12 November 2015.

Müller, T., Laborde, M., Kassel, G., Wiedensolher, A., 2011. Design and performance of a three-wavelenght LED-based total scatter and backscatter integrating nephelometer. Atmos. Meas. Tech. 4, 1291–1303. https://doi.org/10.5194/amt-4-1291-2011.

Nicolás, J.F., Castañer, R., Crespo, J., Yubero, E., Galindo, N., Pastor, C., 2018. Seasonal variability of aerosol absorption parameters at a remote site with high mineral dust loads. Atmos. Res. 210, 100–109. https://doi.org/10.1016/j.atmosres.2018.04.008.

Nicolás, J.F., Castañer, R., Galindo, N., Yubero, E., Crespo, J., Clemente, A., 2019. Analysis of aerosol scattering properties and PM_{10} concentrations at a mountain site influenced by mineral dust transport. Atmos. Environ. 213, 250–257. https://doi.org/10.1016/j.atmosenv.2019.06.017.

Nicolás, J.F., Lucarelli, F., Galindo, N., Yubero, E., Crespo, J., Calzolai, G., Nava, S., 2020. Impacto f traffic flows and meteorological events on the hourly elemental composition of fine and coarse particles at an urban site. Aerosol Air Qual. Res. 20, 991–1001. https://aaqr.org/articles/aaqr-19-09-oa-0437.

Omar, A.H., Won, J., Winker, D.M., Yoon, S., Dubovik, O., McCormick, 2005. Development of global aerosol models using cluster analysis of Aerosol Robotic network (AERONET) measurements. J. Geophys. Res.-Atmos. 110 (10), 10–14. https://doi.org/10.1029/2004JD004874.

Pandolfi, M., Cusack, M., Alastuey, A., Querol, X., 2011. Variability of aerosol optical properties in the Western Mediterranean Basin. Atmos. Chem. Phys. 11, 8189–8203. https://doi.org/10.5194/acp-11-8189-2011.

Pandolfi, M., Alados-Arboledas, L., Alastuey, A., Andrade, M., Angelov, C., Artiñano, B., Backman, J., Baltensperger, U., Bonasoni, P., Bukowiecki, N., Collaud Coen, M., Conil, S., Coz, E., Crenn, V., Dudoitis, V., Ealo, M., Eleftheriadis, K., Favez, O., Fetfatzis, P., Fiebig, M., Flentje, H., Ginot, P., Gysel, M., Henzing, B., Hoffer, A., Smejkalova, A., Kalapov, I., Kalivitis, N., Kouvarakis, G., Kristensson, A., Kulmala, M., Lihavainen, H., Lunder, C., Luoma, K., Lyamani, H., Marinoni, A., Mihalopoulos, N., Moerman, M., Nicolas, J., O'Dowd, C., Petäjä, T., Petit, J.E., Pichon, J.M., Prokopciuk, N., Putaud, J.P., Rodríguez, S., Sciare, J., Sellegri, K., Swietlicki, E., Titos, G., Tuch, T., Tunved, P., Ulevicius, V., Vaishya, A., Vana, M., Virkkula, A., Vratolis, S., Weingartner, E., Wiedensohler, A., Laj, P., 2018. A European aerosol phenomenology – 6: scattering properties of atmospheric aerosol particles from 28 ACTRIS sites. Atmos. Chem. Phys. 18, 7877–7911. https://doi.org/10.5194/acp-18-7877-2018.

Park, M., Joo, H.S., Lee, K., Jang, M., Kim, S.D., Kim, I., Borlaza, L.J.S., Lim, H., Shin, H., Chung, K.H., Choi, Y.-H., Park, S.G., Bae, M.-S., Lee, J., Song, H., Park, K., 2018. Differential toxicities of fine particulate matters from various sources. Sci. Rep. 8, 17007. https://doi.org/10.1038/s41598-018-35398-0.

Prati, P., Zucchiatti, A., Lucarelli, F., Mandó, P.A., 2000. Source apportionment near a steel plant in Genoa (Italy) bycontinuous aerosol sampling and PIXE analysis. Atmos. Environ. 34, 3149–3157. https://doi.org/10.1016/S1352-2310(99)00421-5.

Ran, L., Deng, Z.Z., Wang, P.C., Xia, X.A., 2016. Black carbon and wavelength-dependent aerosol absorption in the North China Plain based on two-year aethalometer measurements. Atmos. Environ. 142, 132–144. https://doi.org/10.1016/j.atmosenv.2016.07.014.

Rizzo, L.V., Correia, A.L., Artaxo, P., Procópio, A.S., Andreae, M.O., 2011. Spectral dependence of aerosol light absorption over the Amazon Basin. Atmos. Chem. Phys. 11, 8899–8912. https://doi.org/10.5194/acp-11-8899-2011.

Romano, S., Perrone, M.R., Pavese, G., Esposito, F., 2019. Optical properties of $PM_{2.5}$ particles: results from a monitoring campaign in southeastern Italy. Atmos. Environ. 203, 35–47. https://doi.org/10.1016/j.atmosenv.2019.01.037.

Schmeisser, L., Andrews, E., Ogren, J.A., Sheridan, P., Jefferson, A., Sharma, S., Kim, J. E., Sherman, J.P., Sorribas, M., Kalapov, I., Arsov, T., Angelov, C., Mayol-Bracero, O. L., Labuschagne, C., Kim, S.-W., Hoffer, A., Lin, N.-H., Chia, H.-P., Bergin, M., Sun, J., Liu, P., Wu, H., 2017. Classifying aerosol type using in situ surface spectral aerosol optical properties. Atmos. Chem. Phys. 17, 12097–12120. https://doi.org/10.5194/acp-17-12097-2017.

Schuster, G.L., Dubovik, O., Holben, B.N., 2006. Ångström exponent and bimodal aerosol size distributions. J. Geophys. Res. 111, D07207 https://doi.org/10.1029/2005JD006328.

Seinfeld, J.H., Pandis, S.N., 2016. Atmospheric Chemistry and Physics: From Air Pollution to Climate Change, Third edition. J. Wiley &Sons, INC.

Shen, Z., Zhang, Q., Cao, J., Zhang, L., Lei, Y., Huang, Y., Huang, R.J., Gao, J., Zhao, Z., Zhu, C., Yin, X., Zheng, C., Xu, H., Liu, S., 2017. Optical properties and possible sources of brown carbon in $PM_{2.5}$ over Xían, China. Atmos. Environ. 150, 322–330. https://doi.org/10.1016/j.atmosenv.2016.11.024.

Szkop, A., Pietruczuk, A., Posyniak, A., 2016. Classification of aerosol over Central Europe by cluster analysis of aerosol columnar optical properties and backward trajectory statistics. Acta Geophys. 64, 2650–2676. https://doi.org/10.1515/acgeo-2016-00112.

Titos, G., Ealo, M., Pandolfi, M., Pérez, N., Sola, Y., Sicard, M., Comerón, A., Querol, X., Alastuey, A., 2017. Spatiotemporal evolution of a severe winter dust event in the western Mediterranean: Aerosol optical and physical properties. J. Geophys. Res. 122, 4052–4069. https://doi.org/10.1002/2016JD026252.

Valentini, S., Barnaba, F., Bernardoni, V., Calzolai, G., Costabile, F., Di Liberto, L., Forello, A.C., Gobbi, G.P., Gualteri, M., Lucarelli, F., Nava, S., Petralia, E., Valli, G., Wiedensohler, A., 2020. Classifying aerosol particles through the combination of optical and physical-chemical properties: results from a wintertime campaign in Rome (Italy). Atmos. Res. 235, 104799. https://doi.org/10.1016/j.atmosres.2019.104799.

Valenzuela, A., Olmo, F.J., Lyamani, H., Antón, M., Quirantes, A., Alados-Arboledas, L., 2012. Classification of aerosol radiative properties during African desert dust intrusions over southeastern Spain by sector origins and cluster analysis. J. Geophys. Res. 117, D06214 https://doi.org/10.1029/2011JD016885.

Weingartner, E., Saathof, H., Schnaiter, M., Streit, N., Bitnar, B., Baltensperger, U., 2003. Absorption of light by soot particles: Determination of the absorption coefficient by means of Aethalometers. J. Aerosol Sci. 34, 1445–1463. https://doi.org/10.1016/S0021-8502(03)00359-8.

WMO/GAW Aerosol Measurement Procedures, 2016. Guidelines and Recommendations, 2nd edition. World Meteorological Organization.

Wu, X., Liu, J., Wu, Y., Wang, X., Yu, X., Shi, J., Bi, J., Huang, Z., Zhou, T., Zhang, R., 2018. Aerosol optical absorption coefficients at a rural site in Northwest China: the great contribution of dust particles. Atmos. Environ. 189, 145–152. https://doi.org/10.1016/j.atmosenv.2018.07.002.

Yang, M., Howell, S.G., Zhuang, J., Huebert, B.J., 2009. Attribution of aerosol light absorption to black carbon, brown carbon, and dust in China – interpretations of atmospheric measurements during EAST-AIRE. Atmos. Chem. Phys. 9, 2035–2050. https://doi.org/10.5194/acp-9-2035-2009.

Zhao, Z., Cao, J., Chow, J., Watson, J.G., Chen, A., Wang, X., Wang, Q., Tian, J., Shen, Z., Zhu, C., Liu, S., Tao, J., Ye, Z., Zhang, T., Zhou, J., Tian, R., 2019. Multi-wavelength light absorption of black and brown carbon at a high altitude site on the Southeastern margin of the Tibetan Plateau, China. Atmos. Environ. 212, 54–64. https://doi.org/10.1016/j.atmosenv.2019.05.035.

Zhu, C.S., Cao, J.J., Hu, T.F., Shen, Z.X., Tie, X.X., Huang, H., Wang, Q.Y., Huang, R.J., Zhao, Z.Z., Moćnik, G., Hansen, A.D.A., 2017. Spectral dependence of aerosol light absorption at an urban and remote site over the Tibetan Plateau. Sci. Total Environ. 590-591, 14–21. https://doi.org/10.1016/j.scitotenv.2017.03.057.